Computations of the Flow Past a Still Sphere at Moderate Reynolds Numbers Using an Immersed Boundary Method

Rubens Campregher
rubenscamp@gmail.com

Julio Militzer
jmilitze@dal.ca
Dalhousie University
Department of Mechanical Engineering
Halifax, NS, Canada

Sérgio Said Mansur
Emeritus Member, ABCM
mansur@dem.feis.unesp.br
São Paulo State University – UNESP
Department of Mechanical Engineering
Ilha Solteira, SP, Brazil

Aristeu da Silveira Neto
Emeritus Member, ABCM
aristeus@mecanica.ufu.br
Federal University of Uberlândia – UFU
School of Mechanical Engineering
Uberlândia, MG, Brazil

This paper presents an immersed boundary formulation for three-dimensional incompressible flows that uses the momentum equation to calculate the Lagrangian force field indirectly imposing the no-slip condition on solid interfaces. In order to test the performance of this methodology the flow past a sphere for Reynolds numbers up to 1,000 have been calculated. Results are compared with numerical data from other authors and empirical correlations available in the literature. The agreement is found to be very good.
Keywords: *immersed boundary method, virtual physical model, flow past sphere, transitional flow*

Introduction

The literature provides several examples of both numerical and experimental analysis of the flow around a stationary sphere – Almedeij (2008), Bouchet et al. (2006), Ploumhans et al. (2002), Howe et al. (2001), Kim et al. (2001), Fadlun et al. (2000), Tomboulides and Orszag (2000), Johnson and Patel (1999), Mittal and Najjar (1999), Fornberg (1988), Shirayama (1992). Despite the geometric symmetry and simplicity of a solid sphere, complex flow patterns can be observed in the wake at moderate large Reynolds numbers, whose characterization constitutes an interesting benchmark for validating Navier-Stokes equations solvers.

The conventional approach to the discretisation and solution of this class of flow is to use spherical coordinates (O-grid type). However, the use of O-grids imposes additional complexity to numerical modelling and restricts the application of the numerical algorithm, since the grid can be applied only to a specific coordinate system.

One alternative to body-fitting meshes is the increasingly popular immersed-boundary (IB) method. The immersed boundary method was pioneered by Peskin (1972) working on the simulation of blood flow through cardiac valves. The author applied the IB method to represent the interaction of the cardiac valve deformable tissue with the viscous flow. Since then, the method has experienced successive refinements and modifications, becoming nowadays an important tool for solving general fluid-fluid or solid-fluid interaction problems. Several different applications of the method are inventoried in recent reviews by Peskin (2002) and Mittal and Iaccarino (2005).

From a conceptual viewpoint the distinguishing quality of IB methods is their ability to simulate the presence of an interface inside the flow by adding a body force field to discretised Navier-Stokes equations source term. The embedded interface is represented by arbitrary Lagrangian points (IB mesh), whereas the flow domain is usually discretised by an Eulerian orthogonal grid. An interpolation function transfers the information from the flow domain to the IB mesh and back. This domain independence allows the IB mesh to easily move and/or deform relatively to the flow mesh. The way the force field term is evaluated and the interpolation function is defined characterizes the different variants of IB formulation.

In the approach used by Peskin (1977) the source of the additional force term was the deformation rate of the elastic immersed boundary whose constitutive points were tied by elastic membranes. A sinusoidal interpolation function was then used to transfer the elastic tension to the fluid body force term, creating the force field. In the work of Lai (1998), higher order discretisation techniques were used to improve the numerical stability of the method. Later on, Roma et al. (1999) introduced adaptive grids and a new interpolation function to the model presented in Peskin (1977).

Unverdi and Tryggvason (1992) have applied the IB methodology to two-phase flows and the force term was evaluated using the interfacial tension. The authors simulated bubbles in both two and three-dimensional domains. For 3D simulations, the line segments that compose the geometry in 2D were substituted by a mesh of triangular elements. The flow domain was discretised using a finite difference method over a staggered grid, with second-order approximation for spatial derivatives and first-order approximation for time derivatives. One of the important contributions of the paper is the use of an indicator function to locate the regions occupied by the fluid-solid interface.

Goldstein et al. (1993) have proposed a function that relates the flow velocity at the interface with the velocity of the interface itself using two *ad hoc* constants. One of the constants produces natural frequency oscillation while the other dampens the response oscillations. This method was named feedback forcing method as the constants are adjusted accordingly to the flow response to the changes imposed by the force term. It is worth mentioning that no interpolation function was used for points inside or outside the geometry. Three-dimensional simulations employing the force feedback method can be found in Goldstein et al. (1995). Saiki and Biringen (1996) have implemented higher-order discretisations of Goldstein's method. The

authors have simulated flows around stationary, rotating, and oscillating cylinders for Reynolds numbers less than 400.

Mohd-Yusof (1997) has proposed that the Lagrangian force field should be evaluated based on the flow momentum equation at the boundary interface without *ad hoc* constants. This method was named direct forcing method. Nonetheless, it requires complex algorithms to locate the geometry inside the flow domain and uses expensive B-spline interpolations to evaluate the flow properties along the interface. Fadlun et al. (2000) have compared the work of Goldstein et al. (1993) and Mohd-Yusof (1997) and concluded that the latter has significant advantages over the former, especially for three-dimensional domains due to less expensive algorithm. Furthermore, the advantage remained unchanged even when the best constants were set on Goldstein's model. The authors also tried to improve the results by increasing the number of iterations within each time step. This procedure was considered unnecessary.

Kim et al. (2001) have performed some experiments using Mohd-Yusof's methodology for domains discretised by the finite volume method. The authors have added source and sink terms to volumes overlapped by the boundary and/or to volumes inside body to help increase the accuracy of the solution. Such procedure has diminished the dependence of the model on the number of interpolation points inside the body as well as the relative distance among them. Gilmanov et al. (2003) have proposed to represent three-dimensional geometries by several distribution and interpolations procedures inside the Cartesian grid. To validate the methodology the authors simulated the flow past a sphere at Reynolds numbers up to 300.

More recently, Lima e Silva et al. (2003) have proposed a model that evaluates the force field by applying the flow momentum equation at the constitutive points of the geometry. Since the model employs the momentum balance equation to calculate the forcing term and indirectly imposes the no-slip condition on the immersed boundary, it was named by the authors Virtual Physical Model (VPM).

The current paper presents a remodelled version of the VPM with an extension to 3D domains. This novel algorithm enables the methodology to represent various physical problems in more realistic conditions, since 3D flows are ubiquitous in geophysical and engineering applications. Considering that accurate 3D unsteady Navier-Stokes calculations require very large memory resources and processing capabilities, the code has parallel processing capabilities and run on a Beowulf cluster. The general concept of the code is delineated in this work, but programming details are omitted and can be found in Campregher (2005). To validate the numerical and computational procedures, the flow past a single rigid sphere was chosen as test case. The Reynolds number varies from 100 to 1,000.

Mathematical Modeling

The Eulerian Domain

The flow domain is discretized with the finite volume method over a non-uniform mesh. The fluid is assumed incompressible and isothermal. Therefore, the Navier-Stokes equation in its integral form becomes:

$$\frac{\partial}{\partial t}\int_{\Omega}\rho\,u_i\,\mathrm{d}\Omega+\int_{S}\rho\,u_i\,v_j\,n_j\,\mathrm{d}S=\int_{S}\tau_{ij}\,n_j\,\mathrm{d}S$$
$$-\int_{S}p\,\delta_{ij}\,n_j\,\mathrm{d}S+\int_{\Omega}f_i\,\mathrm{d}\Omega \tag{1}$$

where f_i is the force field term associated with the volume element

along the direction i, τ_{ij} is the viscous tensor component, and P is the pressure. The time derivative is approximated by the second-order three-time level scheme (Ferziger and Peric, 2002) and the spatial derivatives by the central-difference scheme (CDS). The pressure-velocity coupling is done using the SIMPLEC method (Van Doormal and Raithby, 1984) and the variables are placed in a co-located arrangement. The Rhie-Chow interpolation (Rhie and Chow, 1983) method is used to avoid numerical oscillations due to pressure checkerboard fields. The flux at cell faces is approximated using a deferred-correction algorithm (Ferziger and Peric, 2002) and the upwind interpolation scheme is blended with the CDS by:

$$(F)^n=(F_L)^n+\gamma\,(F_H+F_L)^{n-1} \tag{2}$$

where L and H stand for, respectively, low and high order flux (F) term approximation and n is the current iteration. A value of $\gamma = 1.0$ is used in all computations, leading to CDS dominant interpolation scheme at convergence. The linear systems generated by the discretisation of velocity components are solved by the SOR (Successive Over-Relaxation) algorithm whereas the SIP (Strongly Implicit Procedure) algorithm (Stone, 1968) is used to solve the pressure correction system of equations.

The Virtual Physical Model

The fluid-solid interface is discretised by a mesh of triangular elements. As previously stated, the virtual physical model evaluates the force field by applying the balance of the momentum equations over the Lagrangian points at the boundary. The procedure is done as follows. Let k be a Lagrangian point placed at $\bar{x}_k$ (see Fig. 1) and having velocity u_k.
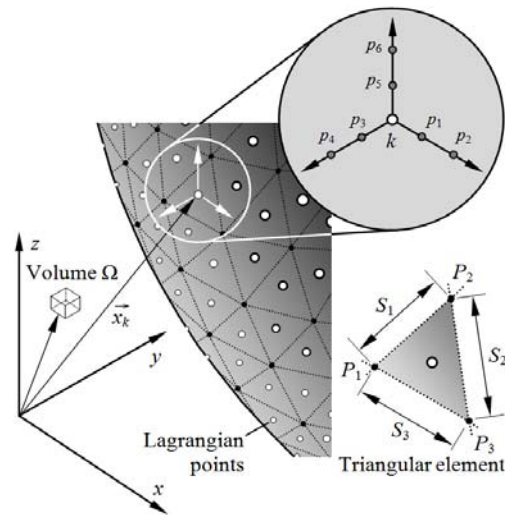

Figure 1. Fluid volume Ω and Lagrangian point k on the fluid-solid interface.

The momentum equation applied over this Lagrangian point (see Campregher, 2005) gives:

$$F_i\,(k)=\frac{\rho\,u_i\,(k)-\rho\,u_i\,(fk)}{\Delta t}-\frac{\partial\left(\rho\,u_j(k)\,u_i\,(k)\right)}{\partial x_j}$$

$$-\mu\left[\frac{\partial}{\partial x_j}\left(\frac{\partial u_i\,(k)}{\partial x_j}\right)\right]+\frac{\partial P(k)}{\partial x_i} \qquad (3)$$

where $F_i(k)$ is the Lagrangian force that changes the velocity $u_i(fk)$ of the fluid particles adjacent to the Lagrangian point k and brings them to the wall velocity, as required by the no-slip condition. The index i represents the directions of the Eulerian coordinate system. The spatial discretisation of Eq. (3) is done by constructing a three-directional axis of reference with origin at k, as shown in Fig. 1. A Lagrangian polynomial is then used to obtain the spatial derivatives. Let m be the number of points employed to construct a polynomial interpolation of order $m-1$. Thus, the value of the component i of the variable ϕ at any point p is given by:

$$\phi_i(p)=\sum_m \psi_m(p)_i\,\phi_m \qquad (4)$$

where:

$$\psi_m(p)_i = \prod_{n,m\neq n}\left(\frac{x_i\,(p)-x_i\,(n)}{x_i\,(m)-x_i\,(n)}\right) \qquad (5)$$

Substituting the points accordingly to the stencil in Fig. 1 the value of ϕ along the x axis (where the points k, p_1, and p_2 lay) can be obtained as:

$$\phi_p=\left[\frac{(x_p-x_{p_1})(x_p-x_{p_2})}{(x_k-x_{p_1})(x_k-x_{p_2})}\right]\phi_k+\left[\frac{(x_p-x_k)(x_p-x_{p_2})}{(x_{p_1}-x_k)(x_{p_1}-x_{p_2})}\right]\phi_{p_1}$$
$$+\left[\frac{(x_p-x_k)(x_p-x_{p_1})}{(x_{p_2}-x_k)(x_{p_2}-x_{p_1})}\right]\phi_{p_2} \qquad (6)$$

Deriving Eq. (6) with respect to the x direction one has:

$$\frac{\partial\phi_p}{\partial x}=\left[\frac{(x_p-x_{p_1})+(x_p-x_{p_2})}{(x_k-x_{p_1})(x_k-x_{p_2})}\right]\phi_k+\left[\frac{(x_p-x_k)+(x_p-x_{p_2})}{(x_{p_1}-x_k)(x_{p_1}-x_{p_2})}\right]\phi_{p_1}$$
$$+\left[\frac{(x_p-x_k)+(x_p-x_{p_1})}{(x_{p_2}-x_k)(x_{p_2}-x_{p_1})}\right]\phi_{p_2} \qquad (7)$$

and the second derivative results:

$$\frac{\partial^2\phi_p}{\partial x^2}=\left[\frac{2\phi_k}{(x_k-x_{p_1})(x_k-x_{p_2})}\right]\phi_k+\left[\frac{2\phi_{p_1}}{(x_{p_1}-x_k)(x_{p_1}-x_{p_2})}\right]\phi_{p_1}$$
$$+\left[\frac{2\phi_{p_2}}{(x_{p_2}-x_k)(x_{p_2}-x_{p_1})}\right]\phi_{p_2} \qquad (8)$$

It is possible to obtain all spatial derivatives required in Eq. (3) by replacing the point p and the variable ϕ in the above Eqs. (6) and (7). If the sides of a triangular element that contains the Lagrangian point k are formed by line segments S_1, S_2, and S_3, connecting the vertex points P_1, P_2, and P_3, that is, $S_1=\overline{P_2\,P_1}$, $S_2=\overline{P_3\,P_2}$, and $S_3=\overline{P_3\,P_1}$, the area ΔA_k of the triangular element is given by:

$$\Delta A_k=\sqrt{S\,(S-S_1)\,(S-S_2)\,(S-S_3)} \qquad (9)$$

where $S=(S_1+S_2+S_3)/2$.

The Distribution Procedure

As aforementioned, the way the force field is evaluated characterizes an immersed boundary method. For the present three-dimensional model the force field is distributed over the Eulerian mesh using Eq. (10):

$$f_i=\sum_k F_i(k)\,D_i\,\Delta A_k\,\Delta S_k \qquad (10)$$

where ΔS_k is the average length of the triangle sides and the distribution function (D_i) is evaluated as:

$$D_i(x_k)=\prod_i\left\{\frac{\varphi\left[(x_k-x_i)/\Delta x_i\right]}{\Delta x_i}\right\} \qquad (11)$$

where the φ function is defined as:

$$\varphi(r)=\begin{cases}\widetilde{\varphi}(r) & if & \|r\|<1\\ \dfrac{1}{2}-\widetilde{\varphi}(2-r) & if & 1<\|r\|<2\\ 0 & if & \|r\|<2\end{cases} \qquad (12)$$

And

$$\widetilde{\varphi}(r)=\frac{3-2\|r\|+\sqrt{1-4\|r\|-4\|r\|^2}}{8} \qquad (13)$$

The distribution function is then divided by a volume unit that cancels out when multiplied by a component of area (ΔA_k) and length (ΔS_k). The Lagrangian force remains as a force density that is integrated over the volume Ω shown in Fig. 1. The interface solid-fluid is represented by an indicator function I evaluated as:

$$\nabla^2 I=\nabla.\,G \qquad (14)$$

where the G function is given by:

$$G=\sum_k D_i\,n_k\,\Delta A_k \qquad (15)$$

where n_k is the normal vector at Lagrangian point k. After the discretisation of Eq. (14), the algebraic equation system is solved using the MSI algorithm (Schneider and Zedan, 1981), which is a variation of the SIP method. For a stationary geometry, the procedure of obtaining the indicator function is carried out only at the beginning of the simulation. Briefly described, the procedure for evaluating the force field in the virtual physical model can be summarized within one outer iteration as:

(i)   After having the solved flow field, the velocity components and the pressure are interpolated to the nearest Lagrangian point k;

(ii) With $u_i(k)$ and $p(k)$, the component of the Lagrangian force $F_i(k)$ is evaluated using Eq. (3);

(iii) The Eulerian force field component associated to a Lagrangian point k is calculated using Eq. (10) over the interface;

(iv) The solution advances in time;

(v)   The force field f_i is added to the source-term of discretised Navier-Stokes equations of the flow field;

(vi) A new flow field is computed and the procedure returns to step (i).

Results and Discussion

The numerical Eulerian domain is detailed in Fig. 2. It has dimensions of 1.0 x 0.68 x 0.68 m and is discretised by 126 x 116 x 116 volumes in x, y, and z directions, respectively. The sphere is discretised by 948 nodes and 1892 triangular elements and has diameter of $D = 0.04$ m and center at $(x_c, y_c, z_c) = (0.38, 0.34, 0.34)$ m. To minimize the influence of the domain walls on the results, the cross sectional area blockage ratio is 0.27%. Also, free-slip boundary condition is imposed on the side walls of the Eulerian domain. The boundary condition for the velocity components at $x = 0$ is $u = U_\infty$, $v = w = 0$. The Reynolds number for the flow past a sphere is defined as:

$$Re = \frac{\rho\, U_\infty\, D}{\mu} \tag{16}$$

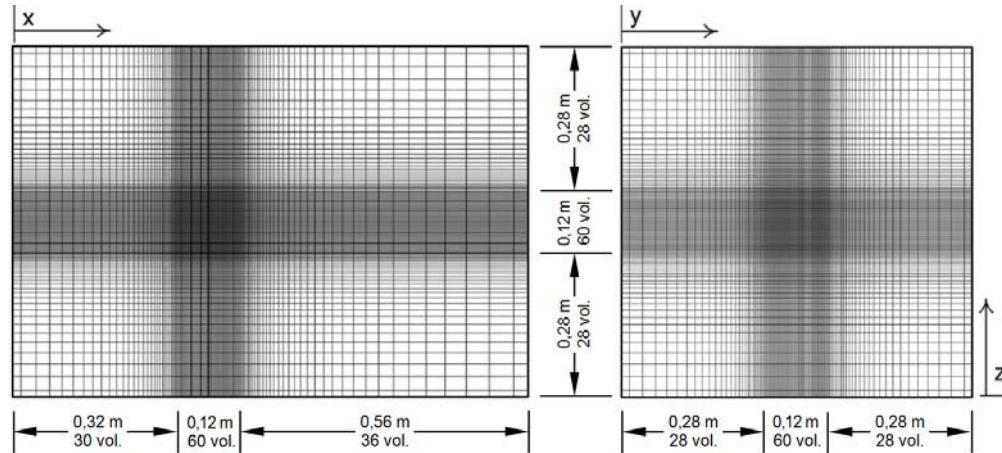where ρ and μ are the fluid density and viscosity, respectively.

Figure 2. Computational mesh (Eulerian domain).

The streamlines for the simulation at $Re = 100$ can be seen in Fig. 3. At this Reynolds number it is possible to observe the two-dimensional behaviour that characterizes laminar flows. The streamlines remain inside a plane that passes through the sphere equator and the recirculation bubbles are symmetric. Such pattern is still unchanged at $Re = 200$ as depicted in Fig. 4 and reported in Gushchin et al. (2002) in which the first instabilities occur within $275 < Re < 295$. It is important to mention that the streamlines deviate correctly from the sphere, as a result of the l_2 norm below 10^{-2} for all Reynolds numbers simulated. This norm has been defined here as the difference between the flow velocity on the interface and the velocity of the interface itself.
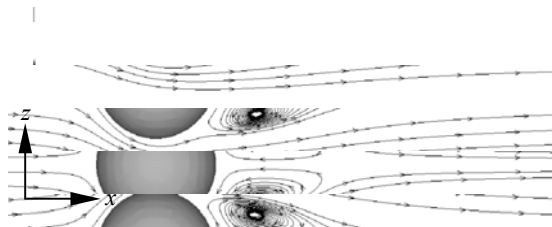
Figure 5 presents the u component of the velocity field along the z axis at $Re = 200$. The important characteristic stressed in Fig. 5 is the zero value of the velocity at the solid-fluid interface. The non-zero velocity profile present inside the geometry is a virtual physical model side effect. It is due to the fact that the methodology uses information from inside as well as outside the boundary to evaluate the forces in the Lagrangian domain. This effect, however, does not affect the results since the flow inside the boundary is also physically consistent.
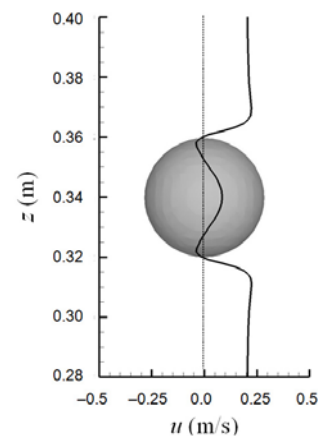

Figure 3. Streamline patterns at $R_e = 100$ (xz plan).
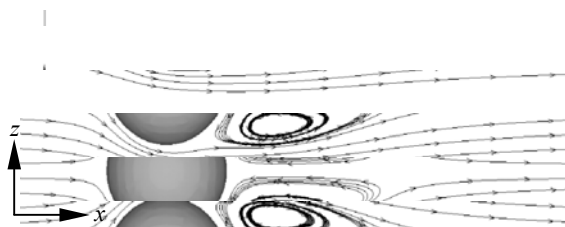
Figure 4. Streamline patterns at $R_e = 200$ (xz plan).

Figure 5. Velocity profile of the component u along the z axis at $R_e = 200$.

The recirculation bubble length (X_S), evaluated from the sphere rear end, provides very useful information about the accuracy of the calculations. The values of X_S were obtained as 0.038 m at $Re = 100$

and 0.056 m at $Re = 200$ and the comparison of the non-dimensional length of the recirculation bubble (X_S/D) with results from the literature are presented in Tab. 1.

Table 1. Non-dimensional recirculation bubble length X_S/D compared with data from literature.

References	$Re = 100$	$Re = 200$
This work	0.94	1.40
Fornberg (1988)	0.87	1.43
Johnson and Patel (1999)	0.88	1.45
Tomboulides and Orszag (2000)	0.87	1.43
Gilmanov et al. (2003)	0.85	1.44

A sequence of hairpin vortices shed behind the sphere at $Re = 400$ can be visualized in Fig. 6 using the Q criterion (Jeong and Hussain, 1995) defined as:

$$Q = \frac{1}{2}\left(\|\Omega\|^2 - \|S\|^2 \right) \tag{17}$$

where:

$$\|S\| = \sqrt{\mathrm{tr}\left(S\, S^T\right)} \tag{18}$$

and

$$\|\Omega\| = \sqrt{\mathrm{tr}\left(\Omega\, \Omega^T\right)} \tag{19}$$

The S and Ω are the symmetric and antisymmetric parts of ∇u, written respectively as:

$$S_{ij} = \frac{1}{2}\left(\frac{\partial u_i}{\partial x_j} + \frac{\partial u_j}{\partial x_i} \right) \tag{20}$$

and

$$\Omega_{ij} = \frac{1}{2}\left(\frac{\partial u_i}{\partial x_j} - \frac{\partial u_j}{\partial x_i} \right) \tag{21}$$

The first picture in Fig. 6 was captured at $\Delta t^* = 140$ and the subsequent frames are separated by $\Delta t^* = 1$. The dimensionless time Δt^* is defined as:

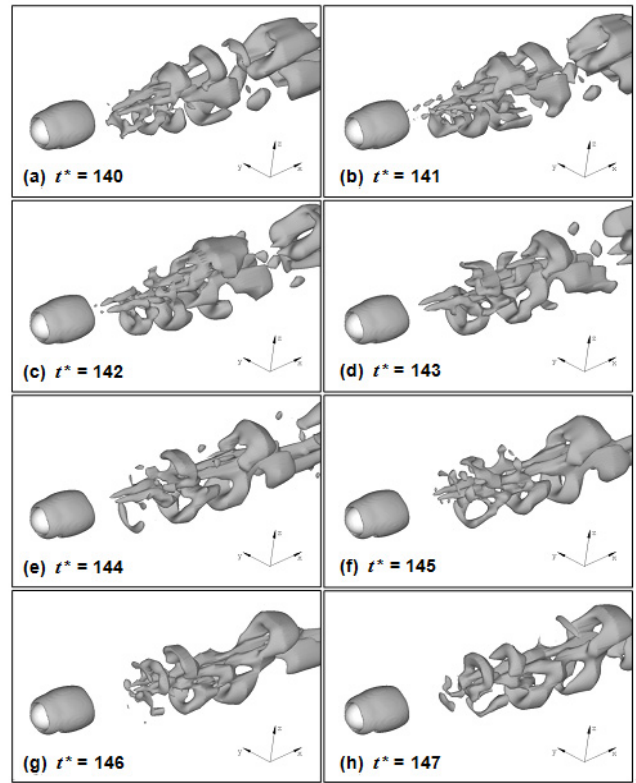$$\Delta t^* = \frac{t\, U_\infty}{D} \tag{22}$$

Figure 6. Temporal sequence of vortex shedding at $Re = 400$.

The toroidal vortices formed alternately around the sphere are shed and eventually deformed due to the difference in flow velocity field along the sphere centerline and the free stream. Such deformation gives origin to pairs of counter-rotating vortices stretched in the streamwise direction. According to Ploumhans et al. (2002), the flow structure shown in Fig. 6 changes again at $Re \cong 420$ resulting in planar symmetry loss and unsteadiness in the vortex shedding frequency. Indeed, Fig. 7 shows that the lift coefficient, given by

$$C_L = \frac{F_z}{\dfrac{1}{2}\,\rho\,U_\infty \left(\dfrac{\pi D^2}{4}\right)}, \tag{23}$$

behaves differently for $Re = 400$ (Fig. 7a) and for $Re = 500$ (Fig. 7b). The drag coefficients results, for all Reynolds numbers simulated, defined as

$$C_D = \frac{F_x}{\dfrac{1}{2}\,\rho\,U_\infty \left(\dfrac{\pi D^2}{4}\right)}, \tag{24}$$

are summarized in Tab. 2. The result of $C_D = 1.178$ for $Re = 100$ is close to $C_D = 1.153$ obtained by Gilmanov et al. (2003), although different from other results presented in Tab. 2. The differences between the results obtained in the present work and the results from the literature are found to be more noticeable at Reynolds numbers 100, 200, and 500. Differences at $Re = 500$ are also reported in other references. Nevertheless, for $Re \geq 400$ the differences barely surpass 1.4% when compared with correlations

found in Subramanian (2003) for $20 \leq Re \leq 260$:

$$C_D = \frac{24}{Re}\left[1 + 0.1935\left(Re^{0.6305}\right)\right] \quad (25)$$

and for $260 < Re \leq 1.5\cdot10^3$:

$$\log_{10} C_D = 1.6435 - 1.1242\left(\log_{10} Re\right) + 0.1558\left(\log_{10} Re\right)^2 \quad (26)$$

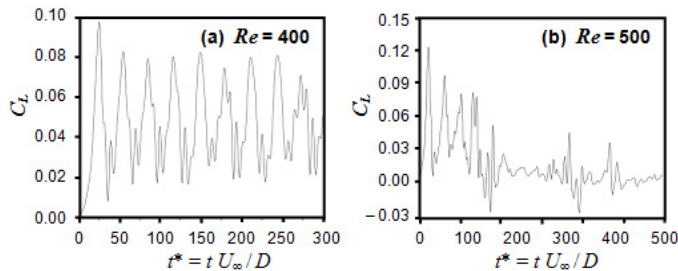Figure 8. Distribution of the probe stations along the sphere wake.

Figure 7. Time evolution of lift coefficient (C_L) for different Re.

Table 2. Drag coefficient compared with data from literature.

Re	[1]	[2]	[3]	[4]	[5]	[6]
100	1.178	1.085	2 1.079	1.087	1.40	1.087
200	0.815	0.7683	0.757	-	1.43	0.776
300	0.675	-	-	0.657	1.45	0.653
400	0.594	-	-	-	1.43	0.594
500	0.520	0.4818	0.476	-	1.44	0.555
600	0.530	-	-	-		0.528
700	0.505	-	-	-		0.508
800	0.495	-	-	-		0.493
900	0.485	-	-	-		0.481
1,000	0.478	0.319	0.321	-		0.471

[1] This work; [2] Fornberg (1988); [3] Fadlun et al. (2000); [4] Kim et al. (2001); [5] Ploumhans et al. (2002); [6] Correlations (25) and (26).

Several numerical probes were inserted into the flow to monitor the time evolution of the velocity field components. The probes (numbered from 1 to 5) were distributed along yz planes named stations. Figure 8 presents five probes placed in a station nD from the rear end of the sphere. The probes were positioned as follows: Probe 1 was placed on the centerline of the sphere, Probes 2 and 3 were placed, respectively, at $-1.5D$ and $+1.5D$ spaced from Probe 1 in y direction, and Probes 4 and 5 were at $-1.5D$ and $+1.5D$ in z direction. The position of Stations A, B, and C can be retrieved by replacing the variable n in Fig. 8 by 1.5, 3, and 4.5, respectively. The signals of the velocity components were acquired at a frequency of 100 Hz.

Figure 9 depicts the results for u velocity (left column), obtained from Station A as well as their Fast Fourier Transforms (right column) at $Re = 500$. The free stream velocity was $U_\infty = 0.5$ m/s and the Strouhal number based on the vortex shedding frequency f was evaluated as:

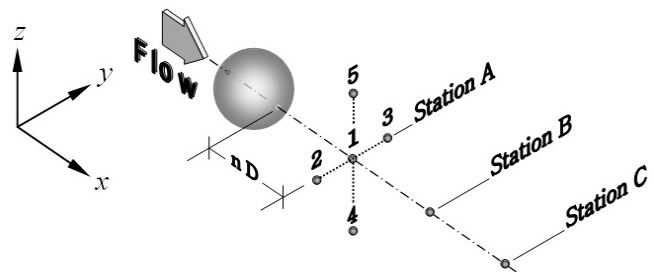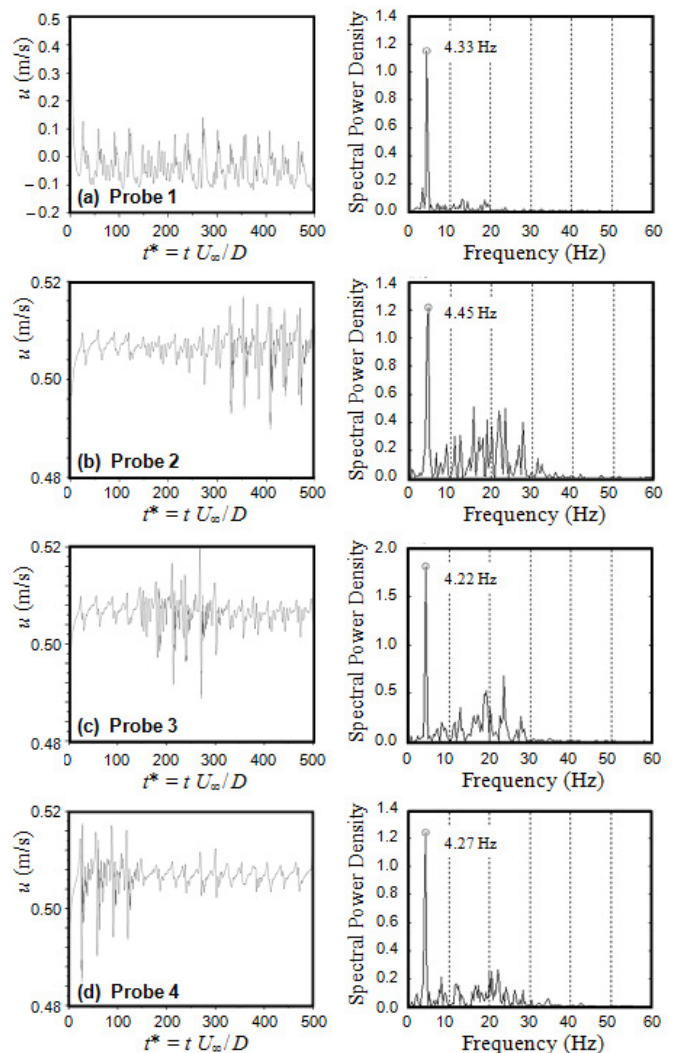$$St = \frac{f\ D}{U_\infty} \quad (27)$$

Figura 9. The u velocity signals (left column) and their Fourier transforms (right column) at $Re = 500$ monitored by the Probes 1, 2, 3, and 4 at the Station A.

It is possible to note that all probes at Station A provide approximately the same main frequency of 4 Hz corresponding to $St = 0.344$. Figure 10 presents the results from probes monitoring the velocity components at $Re = 1,000$. The velocity signals and their Fourier transforms are depicted in the left and right columns, respectively. The free stream velocity was $U_\infty = 1$ m/s and the Strouhal numbers based on the u, v, and w velocity components oscillation frequencies are, respectively, $St = 0.586$, $St = 0.358$, and

St = 0.241. Those results indicate different main frequencies probed at the same place for different velocity components reflecting a non-correlating pattern among them. Thus the flow becomes fully turbulent as reported by Ploumhans et al. (2002) and shown in the Fourier transform plots.
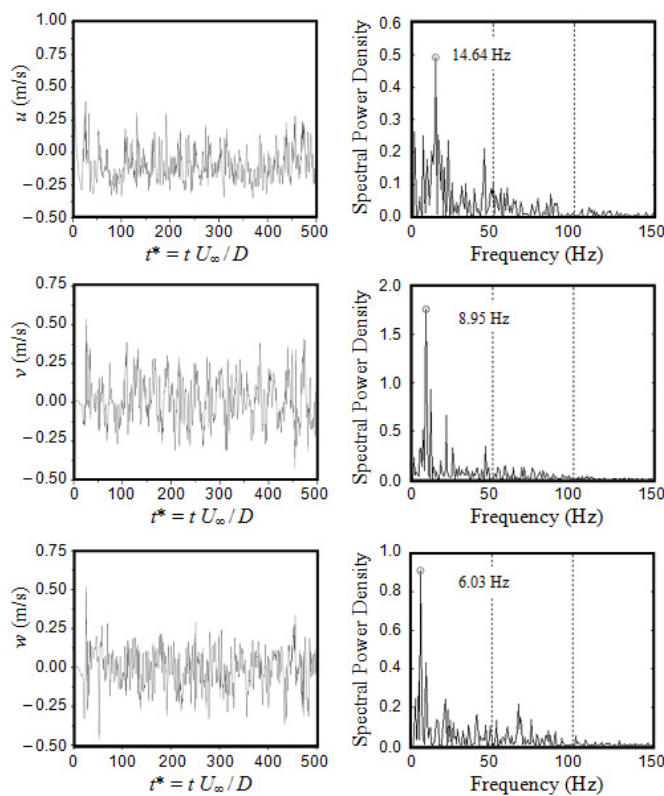

Figura 10. The *u*, *v*, and *w* velocity signals (left column) and their Fourier transforms (right column) at *Re* = 1,000 monitored by the Probe 1 at Station A.

The differences in the Strouhal number suggest a bifurcation pattern in the main frequency above *Re* = 800, as reported by other authors – Tomboulides and Orszag (2000), Mittal and Najjar (1999). Tomboulides and Orszag (2000) obtained, at *Re* = 1,000, *St* = 0.195 and *St* = 0.35 by averaging the frequency of the velocity components data captured at several stations in the near wake. A similar behavior has been reported by Mittal and Najjar (1999) even at lower Reynolds number (*Re* = 650). Therefore, the main frequency obtained for the same flow regime may vary significantly for different experiments.

It is possible to capture the changes in the flow structures topology, from coherent to fully-turbulent, by probing the *u* velocity component at three different stations (A, B, and C) at *Re* = 1,000. The velocity signal was monitored by Probe 1 and is plotted in Fig. 11 (left column), the corresponding Fourier transforms values are in middle column, and the energy spectrum for each frequency in right column. The occurrence of higher energy frequencies occupies a broader range in the abscissa as the monitoring station is placed further downstream. The slope of the spectrum plots approximates the $k^{-5/3}$ behavior according to Kolmogorov's law for fully-developed turbulent flow field.

Conclusion

In this work the flow past a single sphere, with Reynolds number ranging from *Re* = 100 to *Re* = 1,000, has been simulated as a test case for a novel immersed boundary method. The proper deviation of the streamlines around the sphere is very meaningful since the virtual physical method does not directly impose the no-slip condition at the body wall. Instead, a force field is calculated based on the momentum balance equation at Lagrangian points that composes the solid-fluid interface. It has been possible to capture the transition processes, and correspondent critical Reynolds numbers, that characterize this kind of flow. According to Tomboulides and Orszag (2000) and Ploumhans et al. (2002), the first critical Reynolds number occurs at *Re* ≈ 210-212 and it is marked by the instability of the recirculation bubble. For larger *Re*, the vortex structures are shed in a steady pattern, but the flow can no longer be considered axisymmetric. The second critical Reynolds number range *Re* ≈ 270-290 characterizes the unsteadiness of the wake but also shows that the time periodicity and planar symmetry remain (Ploumhans et al., 2002). Finally, the loss of time periodicity and planar symmetry across the flow occur at *Re* ≈ 350-375 (Mittal and Najjar, 1999) or *Re* ≈ 420 (Ploumhans et al., 2002). Several numerical probes have been inserted into the flow to analyze the vortex shedding frequency and turbulent kinetic energy. The ability to reproduce those phenomena suggests that both the algorithm for solving the flow field and the immersed boundary method are not dissipative.

The results for drag coefficient presented very good agreement with the literature, corroborated by a l_2 norm below 10^{-2} for every flow regime simulated. The most significant difference of C_D was observed at *Re* = 500, though this discrepancy is also present in other publications. In Tab. 2 the value of drag coefficients at *Re* = 500 ranges from C_D = 0.476 (Fadlun et al., 2000) to C_D = 0.476 (Ploumhans et al., 2002) and the present result of C_D = 0.520 is close to C_D = 0.503 obtained in Shirayama (1992).

In general, immersed boundary methods are an effective alternative to simulate flow around moving and/or deforming objects, since the transformations are applied only to the set of Lagrangian points that represent the fluid-solid interface. This is a fraction of the computational resources required to rebuild the mesh of an entire domain using the conventional body-fitted approach. Moreover, for the IB method presented here the interface is characterized by a blurred region, which makes the transition between solid and fluid domains smoother. This feature helps alleviate a problem commonly encountered in numerical simulations of moving surfaces: cells located in the solid regions change abruptly into fluid cells, and vice-versa, which may cause numerical instability. On the other hand, the halo around the interface may decrease the accuracy of the solution. However, such a problem also occurs when different grids are used for fluid and solid regions, since a spatial interpolation algorithm has to be devised to transfer information between them.

In particular, the virtual physical model (PVM) has proved to be a promising tool for simulations of three-dimensional flows around complex geometries. Its ability of importing any geometry into a conventional Cartesian grid domain adds flexibility to handle different practical engineering problems. Furthermore, the algorithm was implemented using parallel processing capability which is an important feature when simulating three-dimensional problems. Finally, since there are no *ad hoc* constants to be adjusted, several hours of set up time with a trial and error approach are saved.
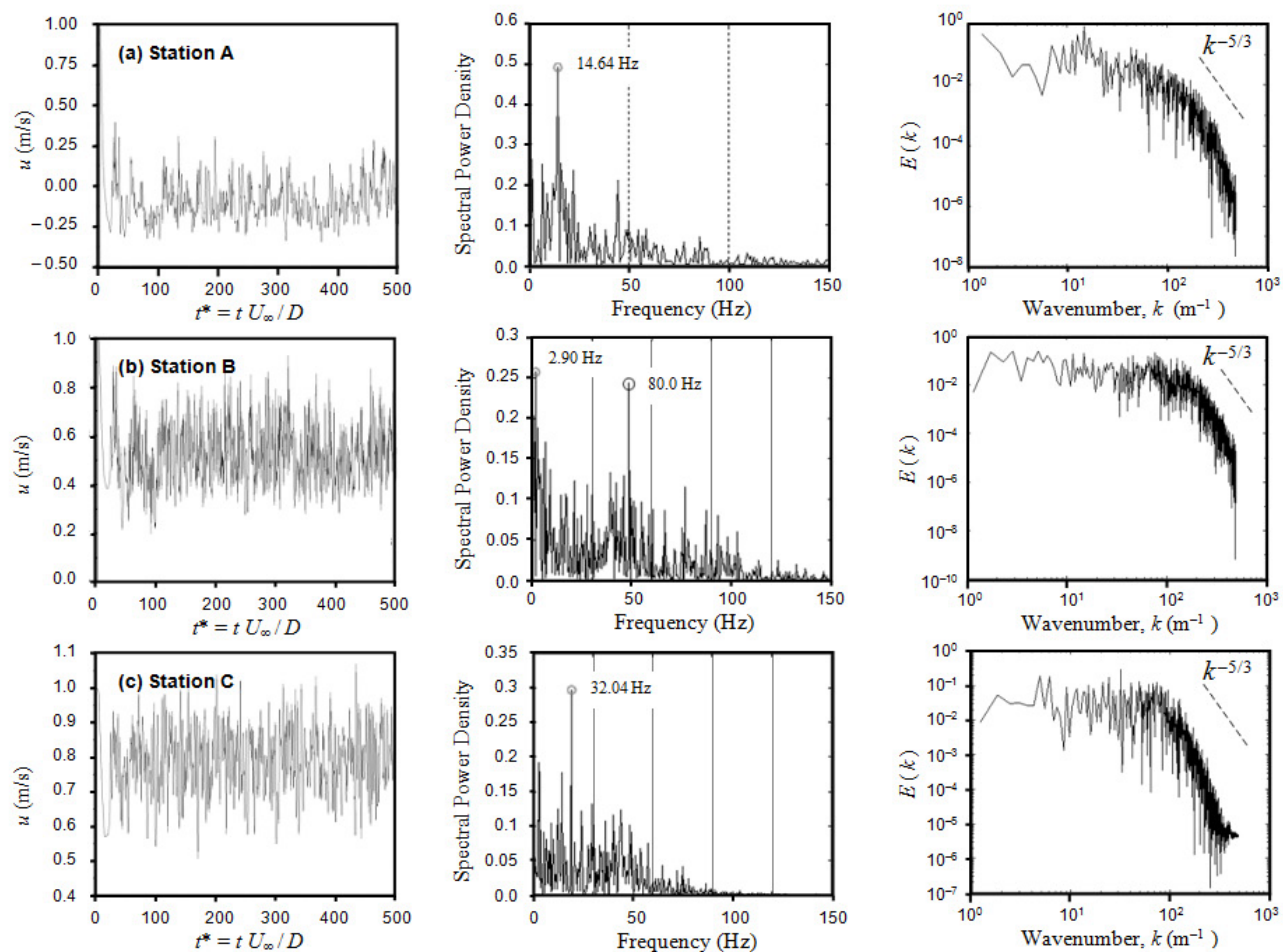
Figure 11. The *u* velocity signals (left column), Fourier transform (middle column), and energy spectrum (right column) at *Re* = 1,000 monitored by the Probe 1 at the Stations A, B, and C.

References

Almedeij, J., 2008, "Drag coefficient of flow around a sphere: matching asymptotically the wide trend", *Powder Technology*, Vol. 186, pp. 218-223.

Bouchet, G., Mebarek, M., Dušek, J., 2006, "Hydrodynamic forces acting on a rigid fixed sphere in early transitional regimes", *European Journal of Mechanics B/Fluids*, Vol. 25, pp. 321-336.

Campregher, R., 2005, "Mathematical Modeling for Three-Dimensional Fluid-Structure Interaction Problems", PhD thesis, Federal University of Uberlandia, Brazil.

Fadlun, E., Verzicco, R., Orlandi, P., Mohd-Yusof, J., 2000, "Combined immersed-boundary finite-difference methods for three-dimensional complex flow simulations", *J. Comp. Phys.*, Vol. 161, pp. 35-60.

Ferziger, J., Peric, M., 2002, "Computational Methods for Fluid Dynamics", 3th ed., Springer-Verlag, New-York, USA.

Fornberg, B., 1988, "Steady viscous flow past a sphere at high Reynolds number", *J. Fluid Mech.*, Vol. 190, pp. 471-489.

Gilmanov, A., Sotiropoulos, F., Balaras, E., 2003, "A general reconstruction algorithm for simulating flows with complex 3D immersed boundaries on Cartesian grids", *J. Comp. Phys.*, Vol. 191, pp. 660-669.

Goldstein, G., Handler, R., Sirovich, L., 1993, "Modeling a no-slip flow boundary with an external force field", *J. Comp. Phys.*, Vol. 105, pp. 354-366.

Goldstein, G., Handler, R., Sirovich, L., 1995, "Direct numerical simulation of the turbulent flow over a modelled ribled covered surface", *J. Fluid Mech.*, Vol. 302, pp. 333-376.

Gushchin, V., Kostomarov, A., Matyushin, P., Pavlyukova, E., 2002, "Direct numerical simulation of the transitional separated fluid flows around a sphere and a circular cylinder", *J. Wind Eng. and Ind. Aerodynamics*, Vol. 90, pp. 341-358.

Howe, M.S., Lauchle, G.C., Wang, J., 2001, "Aerodynamic lift and drag fluctuations of a sphere", *J. Fluid Mech.*, Vol. 436, pp. 41-57.

Jeong, J., Hussain, F., "On the identification of a vortex", *J. Fluid Mech.*, 1995, Vol. 285, pp. 69-94.

Johnson, T.A., Patel, V., 1999, "Flow past a sphere up to a Reynolds number of 300", *J. Fluid Mech.*, Vol. 378, pp. 19-70.

Kim, J., Kim, D., Choi, H., 2001, "An immersed-boundary finite-volume method for simulations of flow in complex geometries", *J. Comp. Phys.*, Vol. 171, pp. 132-150.

Lai, M.C., 1998, "Simulations of the Flow Past an Array of Circular Cylinders as a Test of the Immersed Boundary Method", Ph.D. thesis, New York University, USA.

Lima e Silva, A.L.F., Silveira Neto, A., Damasceno, J.J.R., 2003, "Numerical simulation of two dimensional flows over a circular cylinder using the immersed boundary method", *J. Comp. Phys.*, Vol. 189, pp. 351-370.

Mittal, R., Najjar, F.M., 1999, "Vortex dynamics in the sphere wake", Proc. 30th AIAA Fluid Dynamics Conference, AIAA 99-3806, Norfolk, USA.

Mittal, R., Iaccarino, G., 2005, "Immersed boundary methods", *Annu. Rev. Fluid Mech.*, Vol. 37, pp. 239-261.

Mohd-Yusof, J., 1997, "Combined immersed boundaries/B-splines methods for simulations in complex geometries", CTR Annual Research Briefs, Center for Turbulence Research, NASA Ames/Stanford University, USA, pp. 317-327.

Peskin, C.S., 1972, "Flow patterns around heart valves: a numerical method", *J. Comp. Phys*., Vol. 10, pp. 252-271.

Peskin, C.S., 1977, "Numerical analysis of the blood flow in the heart", *J. Comp. Phys*., Vol. 25, pp. 220-252.

Peskin, C.S., 2002, "The immersed boundary method", *Acta Numerica*, Vol. 11, pp. 479-517.

Ploumhans, P., Winckelmans, G.S., Salmon, J.K., Leonard, A., Warren, M.S., 2002, "Vortex methods for direct numerical simulation of three-dimensional bluff body flows: application to the sphere at *Re* = 300, 500, and 1000", *J. Comp. Phys.*, Vol. 178, pp. 427-463.

Rhie, C., Chow, W., 1983, "Numerical study of turbulent flow past an airfoil with trailing edge separation", *AIAA Journal*, Vol.21, pp.1525-1532.

Roma, A., Peskin, C.S., Berger, M., 1999, "An adaptive version of the immersed boundary method", *J. Comp. Phys.*, Vol. 153, pp. 509-534.

Saiki, E., Biringen, S., 1996, "Numerical simulation of a cylinder in a uniform flow: application of a virtual boundary method", *J. Comp. Phys.*, Vol. 123, pp. 450-465.

Schneider, G.E., Zedan, M., 1981, "A modified strongly implicit procedure for the numerical solution of field problems", *Numer. Heat Transfer*, Vol. 4, pp. 1-19.

Shirayama, S., 1992, "Flow past a sphere: topological transitions of the vorticity field", *AIAA Journal*, Vol. 30, pp. 349-358.

Stone, H.L., 1968, "Iterative solution of implicit approximations of multidimensional partial equations", *SIAM Journal of Numerical Analysis*, Vol. 5, pp. 530-558.

Subramanian, R.S., "Drag on spherical particles and steady settling velocities", note available online at *http://www.clarkson.edu/ subramanian/ch301/notes/index.htm*, pp. 1-3, (accessed 12 June 2007).

Tomboulides, A.G., Orszag, S.A., 2000, "Numerical investigation of transitional and weak turbulent flow past a sphere", *J. Fluid Mech*., Vol. 416, pp. 45-73.

Unverdi, S., Tryggvason, G., 1992, "A front-tracking method for viscous, incompressible multi-fluid flows", *J.Comp. Phys*., Vol. 100, pp. 25-37.

Van Doormal, J., Raithby, G.D., 1984, "Enhancements of the simple method for predicting incompressible fluid flows", *Numerical Heat Transfer*, Vol. 7, pp. 147-163.